A density functional theory study on the interface stability between $CsPbBr_3$ and CuI

Cite as: AIP Advances **10**, 085023 (2020); https://doi.org/10.1063/5.0018925
Submitted: 18 June 2020 . Accepted: 03 August 2020 . Published Online: 19 August 2020

Eric W. Welch, Young-Kwang Jung, Aron Walsh, Luisa Scolfaro, and Alex Zakhidov

A density functional theory study on the interface stability between $CsPbBr_3$ and CuI

Cite as: AIP Advances 10, 085023 (2020); doi: 10.1063/5.0018925
Submitted: 18 June 2020 • Accepted: 3 August 2020 •
Published Online: 19 August 2020

Eric W. Welch,[1,a] Young-Kwang Jung,[2] Aron Walsh,[3] Luisa Scolfaro,[1,4] and Alex Zakhidov[1,4,a]

AFFILIATIONS

[1]Department of Material Science, Engineering and Commercialization, Texas State University, San Marcos, Texas 78666, USA
[2]Department of Materials Science and Engineering, Yonsei University, Seoul 03722, South Korea
[3]Department of Materials, Imperial College London, Exhibition Road, London SW7 2AZ, United Kingdom
[4]Department of Physics, Texas State University, San Marcos, Texas 78666, USA

[a]**Authors to whom correspondence should be addressed:** eric.welch@txstate.edu and alex.zakhidov@txstate.edu

ABSTRACT

This paper assesses the interface stability of the perovskite $CsPbBr_3$ and transport layer CuI using density functional theory and band offset calculations. As a low-cost, more stable alternative to current hole transport materials, CuI may be used to template the epitaxial growth of perovskites such as $CsPbBr_3$ owing to a 1% lattice constant mismatch and larger bulk modulus. We compare all eight atomic terminations of the interfaces between the (100) low-energy facet for both $CsPbBr_3$ and CuI, increasing material thickness to consider charge density redistribution and bonding characteristics between surface and bulk-like regions. A low energy atomic termination is found to exist between these materials where alternating charge accumulation and depletion regions stabilize bonds at the interface. Band offset calculations reveal a type I straddling gap offset in the bulk shifting to a type II staggered gap offset as the thickness of the materials is increased, where the built-in potential changes as layer thickness increases, indicating the tunability of charge separation at the interface. CuI may, thus, be used as an alternative hole transport layer material in $CsPbBr_3$ optoelectronic devices.

I. INTRODUCTION

Hybrid perovskites (HPs) are promising emissive layer materials in optoelectronic devices (OEDs). Their inclusion in photovoltaics,[1–3] light emitting diodes,[4–8] lasers,[9] and photodetectors[10] has revolutionized each respective field. HP OEDs do, however, require the inclusion of charge transport layers to inject/remove requisite mobile electrons/holes, as HPs are intrinsic semiconductors with no majority free charge carrier. The current hole transport layer materials in use, however, are expensive (e.g., Spiro-OMETAD) or acidic (e.g., PEDOT:PSS) and potentially contribute to device instability without added processing steps such as acidity suppression;[11] it should be noted that there are numerous candidates for inexpensive and stable electron transport layer materials. Thus, density functional theory studies on interfaces between perovskites and transport layers may be used to predict stable, efficient materials for HP OEDs.

To combat the high cost and acidity issues inherent in current HP OED transport layer materials, inorganic *p*-type semiconductors such as CuI show promise. This low-cost hole transport layer (HTL) material[12] which is solution-processable at room temperature[13,14] makes direct deposition onto the flexible substrates possible. With a large electronic bandgap (E_g = 3.1 eV),[15] high room-temperature conductivity (σ = 156 S/cm),[16] and high hole mobility ($\mu > 40$ cm^2 V^{-1} s^{-2}),[17] CuI functions well as a HTL in other HP OEDs such as solar cells. CuI has also been shown to improve hole conductivity and air/moisture stability in organic-based, HP devices without decreasing the efficiency.[18] In addition, importantly, cubic γ-phase CuI has a lattice constant (a = 6.05 Å)[19] comparable to that of perovskites such as cubic $CsPbBr_3$ (a = 5.83 Å)[20] with a lattice mismatch of $\frac{\Delta a}{a}$ = 1%, suggesting a possible epitaxial heterointerface with $CsPbBr_3$ grown on CuI. Intuition might suggest CuBr as a replacement transport layer material for a stable, stoichiometric interface, but CuBr is used primarily as a lasing medium in biomedical

applications[21,22] and has a hole conductivity two orders of magnitude smaller than that of CuI.[23]

We report here on density functional theory calculations of the (100) surface energies, interface energies, charge density differences, local potential differences, and valence band offset (VBO) and conduction band offset (CBO) for the novel system of CuI as a HTL in a $CsPbBr_3$ light emitting device. Bond stability and charge redistribution are studied at the surface and interface for all possible terminations. It is noted that defects at HP interfaces and their impact have been reviewed recently[25,26] and are important factors in the accuracy of quantitative studies; however, this is beyond the scope of the current study.

II. CALCULATION METHODS

The bulk 5-atom cubic perovskite and 8-atom cubic zinc-blende γ-phase were used as unit cells for $CsPbBr_3$ and CuI, respectively. Material thickness is increased in the direction normal to the interface (*c*-axis direction) by increasing the number of integer unit cells to study the depth of charge redistribution for each interface. Calculating charge density and local potential difference as a function of material thickness will reveal the type of band offset between the materials.

For all density functional theory calculations, the Vienna *Ab Initio* Simulation Package (VASP)[27–30] with projector augmented wave (PAW)[31,32] pseudopotentials was used with solid revised Perdew–Burke–Ernzerhof (PBEsol)[33] exchange-correlation functionals; range separated hybrid functionals (HSE06) and spin–orbit coupling (SOC) were included in bulk calculations of the total energies. The plane wave basis set for all calculations was truncated at 500 eV with I ($5s^25p^5$), Cu ($3d^{10}4s^1$), Cs ($5s^25p^66s^1$), Pb ($5d^{10}6s^26p^2$), and Br ($4s^24p^5$) orbitals treated as electronic valence states; note that the Pb valence includes d orbital contributions. Core electrons were explicitly treated in the initial state approximation for band-offset calculations to determine the shift between bulk and surface 1s energies for Pb in $CsPbBr_3$ and Cu in CuI; the Pb/Cu 1s energy is averaged for all atoms in the bulk structure and averaged over the bottom three layers for each surface. Gaussian smearing was used to account for partial electronic occupancy with a width in the range of 0.5 meV–1.0 meV, while electronic and ionic relaxation was done with a conjugate gradient line minimization algorithm to relax energies and forces to below 10^{-3} meV/Å and 10^{-2} meV/Å, respectively. Note that the number of electronic bands used during relaxations in surface and interface calculations should be increased by at least 10%–30% of the default value to ensure convergence for larger supercells/surfaces/interfaces; otherwise, the highest band in the calculation may be occupied due to the inclusion of core electrons if there are not a sufficient number of empty virtual orbitals.

To calculate accurate total energies for the interfaces, spin–orbit coupling (SOC) corrections can be used to account for relativistic effects in heavy atoms such as Pb and I, breaking electronic degeneracies near the band edges. In addition, non-local hybrid functionals such as HSE06 can be used to improve the exchange-correlation energy by including a portion of the exact Hartree–Fock exchange, which is over-estimated only using semi-local (PBEsol) functionals. However, in the supercell surface and interface calculations, the addition of these corrections is computationally expensive and, therefore, often prohibitive; therefore, these corrections are only included in the bulk. It is well known, although, that the use of semi-local exchange-correlation alone incorrectly predicts ground state energies in HP systems; however, it has been shown that PBE exchange-correlation still results in significant trends across the data.[34] Defects may also be included and studied using thermochemical models[35] or density functional theory methods,[36] but these are beyond the scope of this study. While quantitative values may be different than the exact experimental ones, it is argued that the band offset and interface stability trends will still be significant using only PBEsol functionals for surface and interface calculations.

The (100) surface for each termination in both $CsPbBr_3$ and CuI was studied, each with at least 15 Å of vacuum between supercell images in surface calculations. Gamma centered k-point meshes were used for all systems with a $6 \times 6 \times 6$ and $10 \times 10 \times 10$ mesh for bulk calculations of $CsPbBr_3$ and CuI, respectively. $6 \times 6 \times 4$, $6 \times 6 \times 3$, $6 \times 6 \times 2$, and $6 \times 6 \times 1$ k-point meshes were used for 1-, 2-, 3-, and 4-unit cells, respectively, for both surfaces and interfaces. Full atomic relaxation was allowed in bulk calculations, while the inner three atomic layers were kept fixed at their bulk location in surface calculations, and only the *c*-axis values were allowed to relax in interface calculations; the cell shape was allowed to relax during interface relaxation calculations, but only the *c*-axis values could move (see the supplementary material for discussion on how to vary only the *c*-axis, keeping the *a*- and *b*-axes constant). The VESTA[37] crystallographic program was used to create atomic geometries and visualize charge density differences, and the MacroDensity[38] (https://github.com/WMD-group/MacroDensity) package was used in post processing for charge density and local potential difference calculations.

The bond cleaving method outlined by Jung *et al.*[24] was for surface and interface calculations. Equation (1) is used to quantify the most stable interface using the energy difference between the relaxed interface and the relaxed surface for each material comprising the interface,

$$E_{intf}(t) = \frac{1}{2A}\left[E^{intf}_{slab}(t) - E^{CsPbBr_3}_{slab}(t) - E^{CuI}_{slab}(t)\right], \quad (1)$$

where *A* is the surface area of the interface, *t* is the surface/interface atomic termination, and the three energy terms are the relaxation total energies of the respective interface/surface for a given termination. As the first term in the brackets is negative for all calculations in this work (see the supplementary material), $E_{intf}(t)$ is negative when the sum of the relaxation total energies of the two composite surface slabs is less than the relaxation total energy of the interface. Thus, the interface with the smallest (most negative) $E_{intf}(t)$ will be the most stable.

III. RESULTS AND DISCUSSION

A Birch–Murnaghan[39] fit to the data (see the supplementary material) reveals a near perfect agreement between experiment and theory for the equilibrium lattice constant in $CsPbBr_3$ (5.88 Å) and a 2% difference between the experimental and theoretical equilibrium lattice constant in CuI (5.95 Å); this discrepancy is attributed to the use of semi-local exchange-correlation functionals in this study. Band gaps calculated at the SOC + HSE06 level of theory are 2.74 eV and 2.83 eV for $CsPbBr_3$ and CuI, respectively. Surface

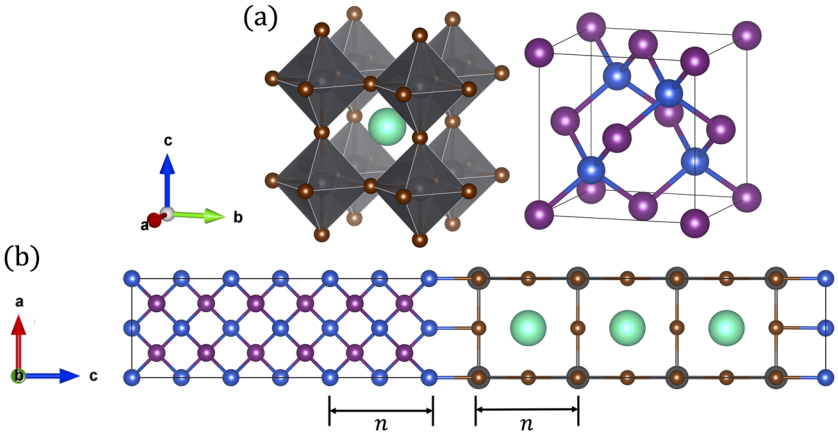

FIG. 1. (a) Structural models of bulk cubic $CsPbBr_3$ and γ-CuI and (b) an interface model with n unit cells replicated. Blue, purple, brown, silver, and green spheres represent Cu, I, Br, Pb, and Cs, respectively.

energy calculations using the bond cleaving method require relaxation energies of slab models. These models are guided by structural properties such as the bulk modulus, which was calculated to be 21.56 GPa and 47.46 GPa for $CsPbBr_3$ and CuI, respectively (Fig. S1). While these values are larger than the experimental values in the literature ($CsPbBr_3$ = 15.5 GPa[40] and CuI = 36.6 GPa[38] experimentally), their relative difference (CuI ~ 2*$CsPbBr_3$) is very close. Relaxed bulk and interface models are shown in Fig. 1, where the number of atomic layers is related to the number of repeated unit cells in the supercell model (n in Fig. 1); images of all eight atomic termination supercells can be seen in Fig. S3.

The surface energy is calculated as the sum of the bond cleaving and surface relaxation energy for each separate system, where the relaxation energy tends to be negative, as shown in Table I; surface models can be seen in Fig. S2. The Cu surface in CuI has a lower surface energy indicating that this surface requires more energy to relax as both Cu and I surfaces, by definition, have the same cleaving energy (see the supplementary material). Surface energy values for the seven atomic layer surface models for both terminations of $CsPbBr_3$ are similar to other works utilizing this method,[24] which are given in parentheses in Table I. The discrepancy between the two sets of data is accounted for due to the different lattice constants between transport layer materials, both of which have larger bulk moduli (PbS a = 5.87 Å and CuI a = 5.95 Å).

Figure 2 shows the charge density redistribution due to an interface for the eight different terminations between CuI and $CsPbBr_3$. A stable interface is indicated both by having the lowest interface energy and by alternating positive (charge accumulation, the yellow isosurface in Fig. 2) and negative (charge depletion, the red isosurface in Fig. 2) charge density regions at the interface. Metal–metal or halide–halide bonding tends to be unstable due to strong Coulombic repulsion indicated by adjacent positive or negative charge density regions; metal–halide bonding is, thus, preferred. For the CsBr layer, due to the orientation of Br/Cs on the corner and Cs/Br in the center, there will always be either a halide–halide bond (I terminated CuI interface) or a metal–metal bond (Cu terminated CuI interface) with CuI; thus, CsBr is not likely to be the growth interface layer. The $PbBr_2$–Cu termination with Br bonded to Cu has the lowest interface energy along with a strong interface interaction (alternating positive and negative charge density regions). This system ($PbBr_2$ termination with Br on the corners and center, all bonded to Cu) is the most likely stable growth interface and is enlarged in Fig. 2 to show the perspective view of the charge density difference. This view shows that all of the Cu bonds are terminated by a Br atom and the Pb atoms sit above the vacant sites in the Cu surface. The charge density redistribution also shows that bulk charge density behavior is recovered within roughly 2–3 atomic layers of the interface in both materials. This indicates that a stable interface exists between $CsPbBr_3$ and CuI (100) surfaces.

To realize the size effects and thickness dependence, the number of layers was increased in each material until the interface energy and band offset converged. Figure 3 illustrates the former case where the greatest change in interface energy occurs when the system thickness increases beyond the bulk system size to 2-unit cells of each material. As the thickness increases, the change in energy decreases and the interface energy converges. Figure 3 also shows that $PbBr_2$ terminated $CsPbBr_3$ on Cu terminated CuI with Br bonding to Cu is the lowest energy interface.

Figure 4 shows the local potential, charge density difference, and band offset calculations for the 4-unit cell interface model of the lowest energy interface. The known methods of analyzing the electrostatic potential[35,39] were used to study the planar averaged potential. The valence band offset (VBO) and conduction band offset (CBO) are given by

$$VBO = \Delta E_v + \Delta V, \quad (2)$$

$$CBO = \Delta E_c + \Delta V, \quad (3)$$

TABLE I. Calculated bond cleaving and surface energies for a 3-unit cell supercell (surface) of CuI and $CsPbBr_3$. Values in parentheses are taken from Ref. 24.

Surface	E_{cl} (meV/Å^2)	E_{rel} (meV/Å^2)	E_{surf} (meV/Å^2)
CuI(100):Cu	51.31	−2.95	48.36
CuI(100):I	51.31	−1.50	49.81
$CsPbBr_3$(100):CsBr	11.49 (10.76)	−5.67 (−5.22)	5.90 (5.54)
$CsPbBr_3$(100):$PbBr_2$	11.49 (10.76)	−3.72 (−3.15)	7.85 (7.61)

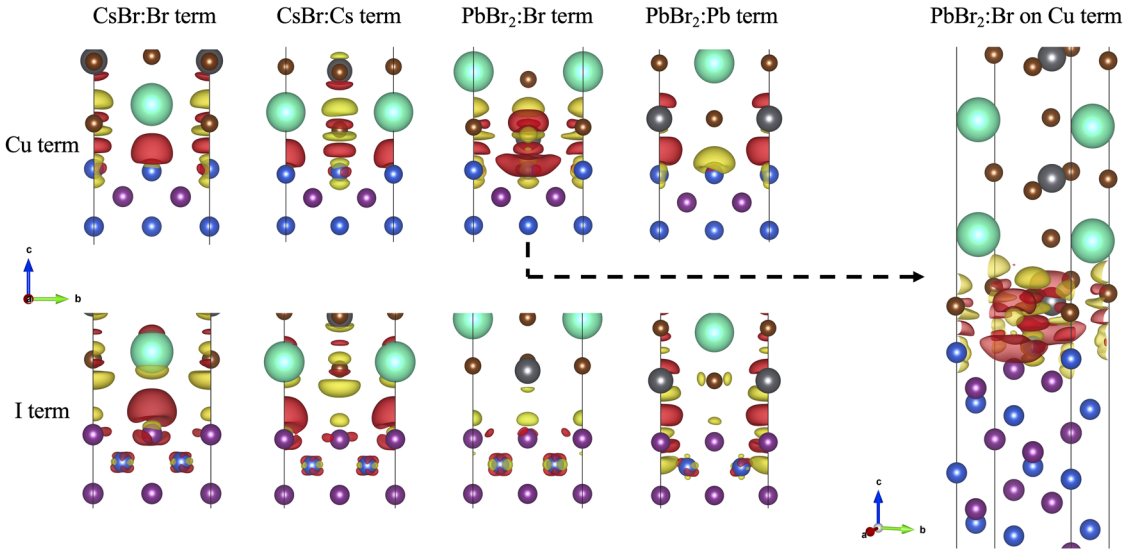

FIG. 2. Charge density difference for each of the eight terminations between $CsPbBr_3$ and CuI viewed along the *a*-axis; columns are labeled by the upper surface termination, while rows are labeled by the lower surface termination. Yellow isosurfaces indicate a region of charge accumulation (positive value), while red isosurfaces indicate a region of charge depletion (negative value). The most stable system (indicated by an arrow) is enlarged and shown from standard orientation on the far right. Blue, purple, brown, silver, and green spheres represent Cu, I, Br, Pb, and Cs, respectively. Isosurface values of 0.003 $e/Å^3$ and 0.0006 $e/Å^3$ were used for Cu and I terminated systems, respectively.

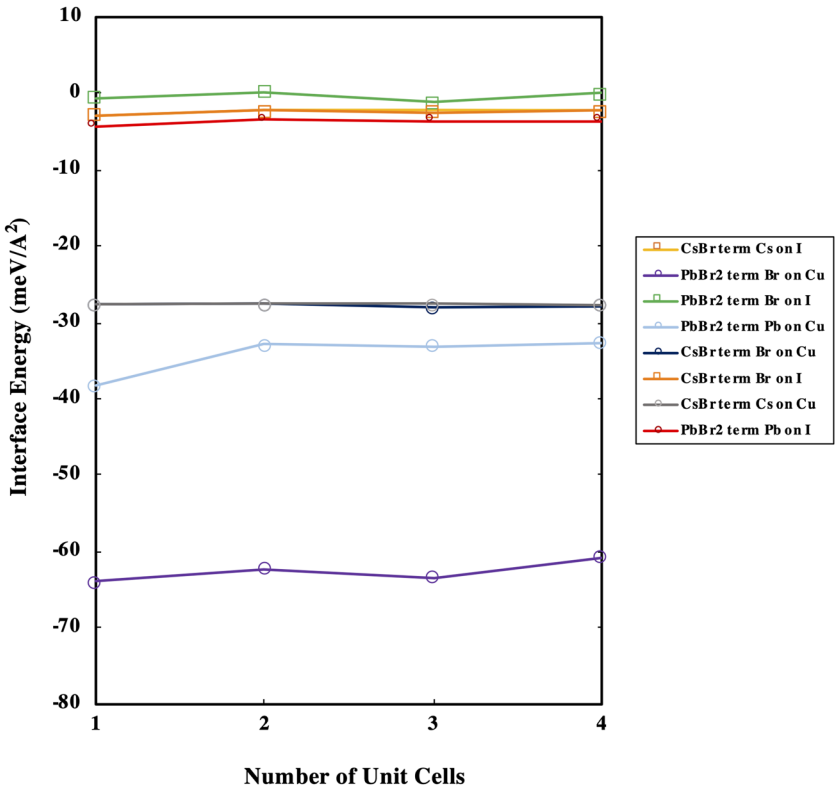

FIG. 3. Interface energy for each atomic termination as a function of layer thickness (the number of integer unit cells). X on Y (i.e., Br on I) indicates that the dominant bonding at the interface occurs between X and Y atoms.

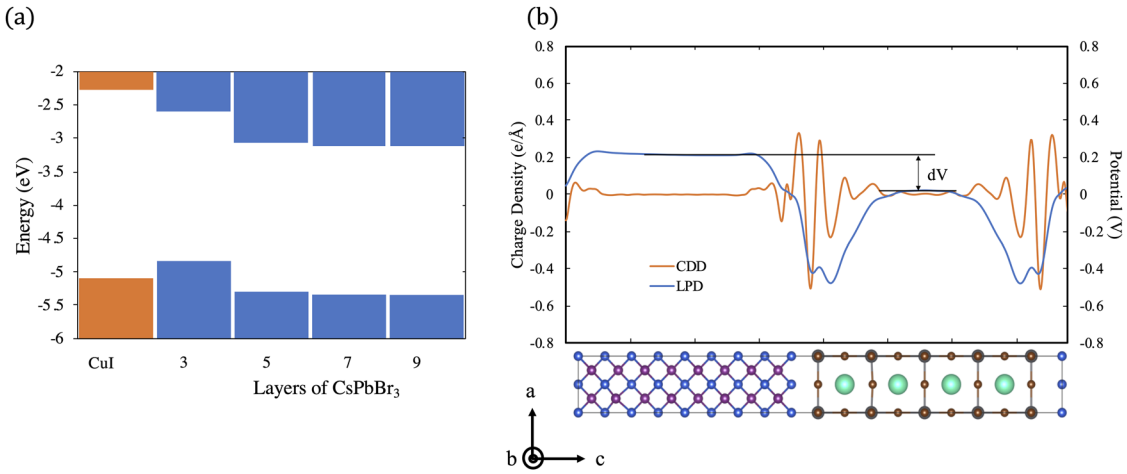

FIG. 4. Analysis of the built-in potential change using (a) band offsets and (b) local potential and charge density difference, revealing a type I offset that changes to a type II staggered gap as material thickness increases, between CuI (orange) and $CsPbBr_3$ (blue) heterostructures and a return to bulk-like behavior within three layers of the interface. The potential dV from band offset calculations is shown in (b) as the difference between the local potential at the center of the two materials. In (b), blue, purple, brown, silver, and green spheres represent Cu, I, Br, Pb, and Cs, respectively.

where $\Delta E_v(\Delta E_c)$ is the difference between absolute energies at the band edges for each material $E_{VBM}(E_{CBM})$ given by

$$\Delta E_v(\Delta E_c) = E^{CsPbBr_3}_{VBM(CBM)} - E^{CuI}_{VBM(CBM)}. \quad (4)$$

Each absolute energy term takes into account the difference between bulk and surface core electron energies, and the vacuum energy of each surface is given by

$$E_{VBM(CBM)} = \varepsilon^{KS}_{VBM(CBM)} - \left(E^{bulk}_{1s} - E^{surf}_{1s}\right) - V_{vac}, \quad (5)$$

where the first term is the Kohn–Sham eigenvalue at the band edge, the terms in the parenthesis are the bulk and surface Pb/Cu 1s energies, and the final term is the vacuum potential for each surface. The potential offset [ΔV, look to Fig. 4(b)] in Eqs. (2) and (3) is the difference between the potential at the center of each material in the interface [plateaus-like in Fig. 4(b)], where bulk-like behavior is restored, and the local potential and charge density differences are nearly zero. The potential offset changes from 1.05 eV in the 1 unit cell interface model to −0.133 eV in the 4 unit cell interface model, indicating that by increasing the thickness of each material, one may modify the charge gradient at the interface to change the direction of charge separation at the interface (see the supplementary material). A type I band offset occurs between unit cell thickness interfaces but changes to a type II offset as the thickness is increased; this is shown in Fig. 4(a) between the materials where the VBO and CBO converge at 4 unit cells of thickness. As the number of layers is increased, the band offset and built-in potential converge with the type II band offset causing holes and electrons to separate at the interface into the two separate materials; convergence is tested as the number of unit cells of each material is increased and is shown in Fig. S4 of the supplementary material.

IV. CONCLUSION

The shift from the type 1 to type II band offset between these two materials indicates charge separation at the interface as the material thickness is increased, where the potential offset may be tuned through controlling layer thickness. Band offsets converge within 4-unit cells of thickness in each material, and bulk behavior is restored within three atomic layers of the interface. The small lattice strain between $CsPbBr_3$ and CuI indicates a stable heterojunction, with the growth of $CsPbBr_3$ guided by the lattice parameters and crystal structure of CuI. A low energy interface exists between $CsPbBr_3$ and CuI indicated both by low interfacial energy and by alternating charge density regions between the Cu–Br bonds at the interface. The most drastic change in the electronic structure occurs as the system transitions from a low-dimensional/extremely thin-film structure such as nanowires to a thicker material such as traditional thin films, indicating that electronic parameters may be tuned by varying material thickness. By carefully controlling the thickness of each material during growth, CuI may, thus, be used as a viable transport layer in $CsPbBr_3$ based optoelectronic devices as a low-cost alternative to current technologies.

SUPPLEMENTARY MATERIAL

See the supplementary material for bulk modulus calculations, slab models, interface models, surface energy calculations, local potential and charge density difference plots, and offset calculations.

ACKNOWLEDGMENTS

E.W.W. and A.Z. acknowledge the Los Alamos National Lab, Center for Integrated Nanotechnology, for access to the Badger HPC cluster and Shane Flaherty at the LEAP HPC cluster at Texas

State University where the majority of calculations were performed. This project was in part funded by the U.S. Department of the Navy, HBCU/MI program, Grant No. N000141912576, and the National Science Foundation, EPMD, Grant No. 1906492. Y.-K.J. and A.W. acknowledge the National Research Foundation of Korea (NRF) grant funded by the Korean government (MSIT) (Grant No. 2018r1c1b6008728).

DATA AVAILABILITY

The data that support the findings of this study are available from the corresponding author upon reasonable request.

REFERENCES

[1] B. Akbali, G. Topcu, T. Guner, M. Ozcan, M. M. Demir, and H. Sahin, Phys. Rev. Mater. **2**, 034601 (2018).
[2] M. A. Green, Y. Hishikawa, E. D. Dunlop, D. H. Levi, J. Hohl-Ebinger, A. W. Y. Ho-Baillie, and A. W. Y. Ho-Baillie, Prog. Photovoltaics **26**, 3 (2018).
[3] R. E. Beal, D. J. Slotcavage, T. Leijtens, A. R. Bowring, R. A. Belisle, W. H. Nguyen, G. F. Burkhard, E. T. Hoke, and M. D. McGehee, J. Phys. Chem. Lett. **7**, 746 (2016).
[4] W. S. Yang, B.-W. Park, E. H. Jung, N. J. Jeon, Y. C. Kim, D. U. Lee, S. S. Shin, J. Seo, E. K. Kim, J. H. Noh, and S. I. Seok, Science **356**, 1376 (2017).
[5] H. Yu, G. Tian, W. Xu, S. Wang, H. Zhang, J. Niu, and X. Chen, Front. Chem. **6**, 1 (2018).
[6] J. Li, L. Xu, T. Wang, J. Song, J. Chen, J. Xue, Y. Dong, B. Cai, Q. Shan, B. Han, and H. Zeng, Adv. Mater. **29**, 1 (2017).
[7] L. Zhang, X. Yang, Q. Jiang, P. Wang, Z. Yin, X. Zhang, H. Tan, Y. M. Yang, M. Wei, B. R. Sutherland, E. H. Sargent, and J. You, Nat. Commun. **8**, 1 (2017).
[8] X. Zhang, B. Xu, J. Zhang, Y. Gao, Y. Zheng, K. Wang, and X. W. Sun, Adv. Funct. Mater. **26**, 1 (2016).
[9] K. Wang, S. Wang, S. Xiao, and Q. Song, Adv. Opt. Mater. **6**, 1800278 (2018).
[10] X. Wang, M. Li, B. Zhang, H. Wang, Y. Zhao, and B. Wang, Org. Electron. **52**, 172 (2018).
[11] M. Kim, M. Yi, W. Jang, J. K. Kim, and D. H. Wang, Polymers **12**, 129 (2020).
[12] S. Ameen, M. S. Akhtar, H. Shin, and M. K. Nazeeruddin, *Advances in Inorganic Chemistry* (Elsevier, 2018), pp. 1–62.
[13] W.-Y. Chen, L.-L. Deng, S.-M. Dai, X. Wang, C.-B. Tian, X.-X. Zhan, S.-Y. Xie, R.-B. Huang, and L.-S. Zheng, J. Mater. Chem. A **3**, 19353 (2015).
[14] W. Sun, H. Peng, Y. Li, W. Yan, Z. Liu, Z. Bian, and C. Huang, J. Phys. Chem. C **118**, 16806 (2014).
[15] J. Zhu, R. Pandey, and M. Gu, J. Phys.: Condens. Matter **24**, 1 (2012).
[16] C. Yang, M. Kneiβ, M. Lorenz, and M. Grundmann, Proc. Natl. Acad. Sci. U. S. A. **113**, 12929 (2016).
[17] D. Chen, Y. Wang, Z. Lin, J. Huang, X. Chen, D. Pan, and F. Huang, Cryst. Growth Des. **10**, 2057 (2010).
[18] J. A. Christians, R. C. M. Fung, and P. V. Kamat, J. Am. Chem. Soc. **136**, 758 (2014).
[19] S. Hull and D. A. Keen, Phys. Rev. B **50**, 5868 (1994).
[20] J. Chen, D. J. Morrow, Y. Fu, W. Zheng, Y. Zhao, L. Dang, M. J. Stolt, D. D. Kohler, X. Wang, K. J. Czech, M. P. Hautzinger, S. Shen, L. Guo, A. Pan, J. C. Wright, and S. Jin, J. Am. Chem. Soc. **139**, 13525 (2017).
[21] S. E. McCoy, Lasers Surg. Med. **21**, 329 (1997).
[22] R. K. Kim, T. Lee, S. Lee, J. Kim, H. Eun, and Y. Huh, J. Korean Phys. Soc. **64**, 755 (2014).
[23] J.-L. Seguin, M. Bendahan, G. Lollmun, M. Pasquinelli, and P. Knauth, Thin Solid Films **323**, 31 (1998).
[24] Y.-K. Jung, K. T. Butler, and A. Walsh, J. Phys. Chem. C **121**, 27351 (2017).
[25] T. H. Han, S. Tan, J. Xue, L. Meng, J. W. Lee, and Y. Yang, Adv. Mater. **31**, 1 (2019).
[26] P. Schulz, D. Cahen, and A. Kahn, Chem. Rev. **119**, 3349 (2019).
[27] G. Kresse and J. Hafner, Phys. Rev. B **47**, 558 (1993).
[28] G. Kreese and J. Hafner, Phys. Rev. B **49**, 14251 (1994).
[29] G. Kresse and J. Furthmüller, Phys. Rev. B **54**, 11169 (1996).
[30] G. Kresse and J. Furthmüller, Comput. Mater. Sci. **6**, 15 (1996).
[31] P. E. Blöchl, Phys. Rev. B **50**, 17953 (1994).
[32] G. Kreese and D. Joubert, Phys. Rev. B **59**, 1758 (1999).
[33] J. P. Perdew, A. Ruzsinszky, G. I. Csonka, O. A. Vydrov, G. E. Scuseria, L. A. Constantin, X. Zhou, and K. Burke, Phys. Rev. Lett. **100**, 136406 (2008).
[34] A. J. Neukirch, I. I. Abate, L. Zhou, W. Nie, H. Tsai, L. Pedesseau, J. Even, J. J. Crochet, A. D. Mohite, C. Katan, and S. Tretiak, J. Phys. Chem. Lett. **9**, 7130 (2018).
[35] Y. Rakita, I. Lubomirsky, and D. Cahen, Mater. Horiz. **6**, 1297 (2019).
[36] D. Meggiolaro and F. De Angelis, ACS Energy Lett. **3**, 2206 (2018).
[37] K. Momma and F. Izumi, J. Appl. Cryst. **41**, 653 (2008).
[38] K. T. Butler, C. H. Hendon, and A. Walsh, J. Am. Chem. Soc. **136**, 2703 (2014).
[39] F. Birch, Phys. Rev. **71**, 809 (1947).
[40] Y. Rakita, S. R. Cohen, N. K. Kedem, G. Hodes, and D. Cahen, MRS Commun. **5**, 623 (2015).